The effect of oil shale ash and basalt-boron fiber on waste package gamma-radiation shielding properties

Hando Tohver[a,*], Andrius Slavickas[b], Maryna Holiuk[c], Andrejs Krasnikovs[d], Riho Mõtlep[e], Iveta Nováková[f], Egidijus Babilas[b], Volodymyr Gulik[a,c]

[a] Institute of Physics, University of Tartu, W. Ostwaldi 1, 50411, Tartu, Estonia

[b] Lithuanian Energy Institute, Breslaujos st. 3, LT-44403, Kaunas, Lithuania

[c] Institute for Safety Problems of Nuclear Power Plants, 12 Lysogirska St, 03028 Kyiv, Ukraine

[d] Department of Theoretical Mechanics and Strength of Material, Riga Technical University, Kipsalas str. 6B, LV-1048, Riga, Latvia

[e] Institute of Ecology and Earth Sciences, University of Tartu, Juhan Liivi 2, 50409 Tartu, Estonia

[f] Department of Construction, Energy and Material Technology, The Arctic University of Norway, Lodve Langesgate 2, 8514, Narvik, Norway

[*] Corresponding author (hando.tohver@ut.ee)

Highlights

- Excellent agreement between Monte Carlo codes
- The container surface dose remained well within limit values
- Additives can be added without limit from radiation protection point of view
- Dose rate distribution mapping provided insight on potential dose hotspots

Abstract

Oil shale ash is an abundant industrial residue that contains hydration products, which have been shown to immobilize heavy metals. The use of innovative additives such as oil shale ash (OSA) and basal-fiber materials containing boron (BBF) have not been thoroughly investigated. This study analyzes the potential of OSA-BBF concrete as an overpack material for low- and intermediate-level radioactive waste containers. Monte Carlo analysis showcases OSA-BBF concrete's superior radiation shielding capability over conventional cement paste. Over a comprehensive 20-year dose rate assessment, OSA-BBF concrete meets the safety standards. The dose rate was not notably sensitive to the amount of additives, meaning they can be added without limit from radiation protection point of view. By investigating the application of oil shale ash in radiation shielding, this research underscores the pathway toward more effective and safer radioactive waste management practices through innovative material choices using recycled industrial residues.

Keywords:

LILW waste packaging, Monte Carlo, Oil shale ash, Basalt-Boron fibers, Cementitious materials

1. Introduction

Cement-based concretes are extensively used for managing various levels of radioactive waste due to their low cost and high density, offering excellent radiation shielding properties alongside the ability to immobilize waste. Although numerous concrete recipes have been investigated for this purpose, the potential of oil shale ash (OSA) remains overlooked (Li et al., 2021). OSA, a largely unused and abundant residue from oil shale power plants demonstrates qualities suitable as an additive in concrete waste packaging material. Its richness in hydration products like calcium-silicate-hydrate gels, ettringite, and monosulfate showcases an ability to immobilize heavy metals (Leben et al., 2019; Ochs et al., 2015).

Concrete can be modified to increase its effectiveness in shielding against radiation by adding various additives, which can either enhance or diminish the strength of the concrete as well as improve the overall durability. In the case of fiber additives, the reinforced concrete can showcase improved mechanical properties, such as increased resistance to cracking. By incorporating radiation-shielding additives into the fibers, for example neutron absorbing boron, the additives can have a larger effect on the shielding properties of the concrete. These developments are supported by previous studies that have shown the viability of basalt-boron fiber additives as a reinforcement for concrete (Skarżyński, 2020).

Most studies focus solely on the radiation shielding properties of cementitious materials without considering their practical application. Models primarily mirror experimental setups, aiming to validate material suitability for radiation-related use (Nabil et al., 2023; Soni et al., 2021). However, without a predefined practical application in mind, these materials may not transition into real-world usage. In the study of radioactive waste containers, the material of the container is often in the center of focus (Han et al., 2018). Improving container materials is important; the container acts as a critical buffer between the processed waste and the surrounding environment. However, it must be noted that for the very same reason, the container material properties are strictly regulated (IAEA-TECDOC-1515, 2006) and it is difficult to transition the material investigations into actual use-cases for the industry.

Most low- and intermediate level waste (LILW) packages are designed to have another

buffer between the waste and external container walls. The waste drums are grouted in place to stop the movement of drums and inhibit the movement of radionuclides to the environment. In the case of container failure, grout serves to limit the movement of groundwater near the waste drums. Oftentimes, a simple recipe of cement paste is used (Nuclear Waste Services, 2022). There are significantly less stringent requirements set for the overpack material as it is surrounded by the container material on all sides. One implicit requirement for the overpack is the package surface dose rate limit, which is defined as 2 mSv/h by the regulations of the Republic of Lithuania (Vaidotas, 2013; Nuclear Waste Services, 2022). In addition, a good overpack material must be leach-resistant and minimize cracking as the latter can be a conduit for radionuclide migration (OECD/NEA, 2012).

In this study, a novel oil shale ash (OSA) and basalt-boron fiber (BBF) concrete has been developed to be used in radioactive waste containers. The study investigates the impact on the radiation shielding properties of using OSA-BBF concrete as an overpack material. By combining oil shale ash with basalt-boron fibers, the structural stability of the overpack can be improved, making it more resistant to micro-cracking. It is known that adding fiber to concrete reduces the level of microcracks in concrete and, as a result, contributes to its durability. Basalt fiber is an eco-friendly material produced from natural basalt rock. The use of basalt fiber as an additive to concrete allows the creation of a new eco-friendly concrete composite material for the nuclear industry (Ipbüker et al., 2015). Modified basalt fiber (infused with boron) increases the neutron radiation shielding properties of concrete and reduces radiation safety issues for the personnel (Zorla et al., 2017).

The investigation methodology, which is based on Monte Carlo codes, has already been demonstrated and validated in a previous paper (Tohver et al., 2024). Preliminary radiation shielding properties of OSA-BBF concrete were also published using a simplified model setup. In this study, a LILW package geometry and waste from the Ignalina Nuclear Power Plant (INPP) was modeled using Monte Carlo codes. The models were used to assess the flux in all package regions, which were converted to whole body effective dose evaluations.

2. Methodology

The evaluation of new overpack materials was done using computer modeling. 5 different Monte Carlo radiation transport codes (OpenMC, EGSnrc, SCALE, Serpent, and MCNP) were used in tandem. The exact parameters, setup of each code, and underlying interactions of OSA-BBF concrete with gamma-radiation have already been described in detail and thoroughly benchmarked in a previous paper (Tohver et al., 2024). This paper will focus on modeling the application of OSA-BBF concretes and their impact on resulting internal and external whole body effective doses.

2.1. Model geometry

This study focused on the waste management practices employed at the Ignalina Nuclear Power Plant in Lithuania. One reason for this is the abundance of oil shale ash in the Baltic region, due to extensive usage of oil shale for electricity generation. The main waste container used for low- and intermediate-level waste (LILW) is constructed from concrete and developed by Framatome-ANP (F-ANP). The container has a maximum waste drum capacity of 8 and will be used for the final disposal of radioactive waste.

To construct a representation of the F-ANP waste package, the physical waste container was simplified, keeping only the primary components of the waste package. The package model included a basic description of the concrete container by modeling four concrete walls, a floor as well as a lid. Since the values of interest were dose rates at the side of the containers, and the containers are designed to be stacked upon one another, a detailed lid description was omitted for a simple slab approach. An illustration of the created model geometry can be found in Fig. 1.

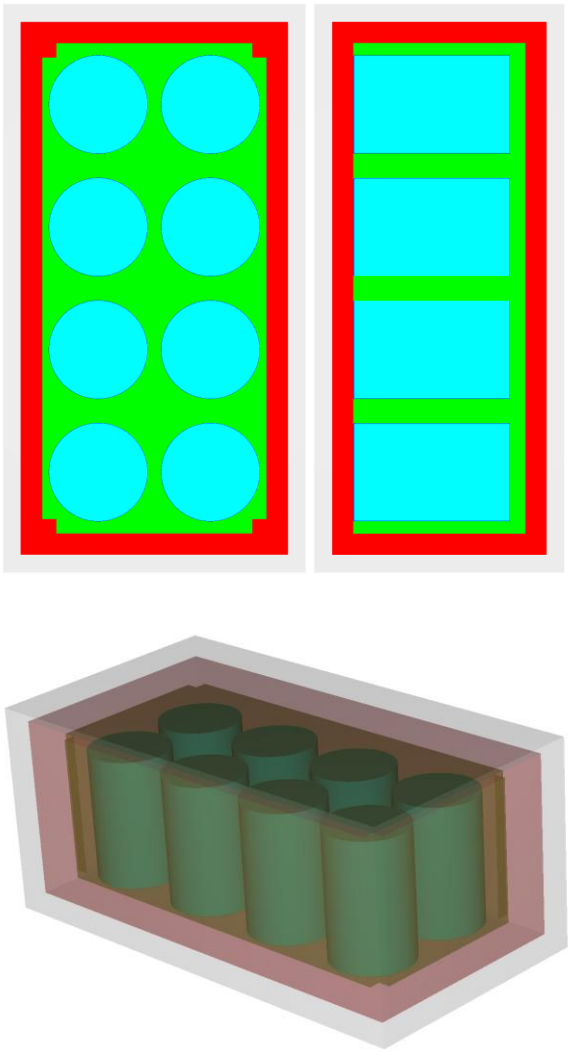

Figure 1: Top-, side-, and isometric view of Framatome-ANP waste package geometry visualized using EGSVIEW.

The waste drums were modeled as 200 L cylinders with different bottom, top and side thicknesses. The drums were placed equidistant from one another. The distance from the outermost drums to the walls was half of the distance between the drums. The drums were surrounded by an overpack material. The overpack material filled the space between the waste drums and the concrete container. Finally, the container was immersed in air to accurately assess the external effective dose rates. The thickness of the container walls was 12 cm, surrounded by 10 cm of air. More information on the dimensions and structure of the

waste container, overpack and drums can be found in the literature (Vaidotas, 2013).

2.2. Material description

This study focused on investigating the impact of waste container overpack materials on the effective dose rates. The container model was constructed of five materials: waste matrix, drum lining, overpack, container structure, and air. Materials other than the overpack were not modified in any way, their chemical composition was kept constant throughout the investigations. Their characterization can be found in Table 1.

Table 1: Densities (g/cm^3) and elemental weight fractions of secondary model materials.

	Waste Matrix	Drum Lining	Container Material	Air, Dry Near Sea Level
Densities (g/cm^3)				
ρ	1.65	7.872	2.3	0.001205
Elemental weight fractions				
H	2.985E-02	0.000E+00	1.000E-02	0.000E+00
C	0.000E+00	5.000E-03	1.000E-03	1.240E-04
N	0.000E+00	0.000E+00	0.000E+00	7.553E-01
O	5.112E-01	0.000E+00	5.291E-01	2.318E-01
Na	3.647E-03	0.000E+00	1.600E-02	0.000E+00
Mg	8.836E-03	0.000E+00	2.000E-03	0.000E+00
Al	3.216E-02	0.000E+00	3.387E-02	0.000E+00
Si	9.037E-02	0.000E+00	3.370E-01	0.000E+00
P	0.000E+00	4.000E-04	0.000E+00	0.000E+00
S	5.126E-03	5.000E-04	0.000E+00	0.000E+00
Ar	0.000E+00	0.000E+00	0.000E+00	1.283E-02
K	3.196E-03	0.000E+00	1.300E-02	0.000E+00
Ca	2.946E-01	0.000E+00	4.400E-02	0.000E+00
Ti	1.214E-03	0.000E+00	0.000E+00	0.000E+00

Mn	0.000E+00	9.000E-03	0.000E+00	0.000E+00
Fe	1.962E-02	9.851E-01	1.400E-02	0.000E+00

The waste stored in the F-ANP containers at the Ignalina Nuclear Power Plant is categorized as either Class B or C level waste. Class B waste includes short-lived low- and intermediate-level waste with surface dose rates between 0.5 - 2 mSv/h, while waste is categorized as Class C when the dose rate is higher than 2 mSv/h. The majority of the waste is made of cemented ion exchange resins, perlite and evaporated concentrate sludge. Three types of mixtures are used for producing the cement matrices: Common Treatment (CT), Separate Resin/Perlite Treatment (SRT) and Separate Concentrate/Perlite Treatment (SCT). Out of these, the CT mixture was chosen as more detailed information was available compared to other mixtures (Vaidotas, 2013). The main components of the waste matrix were cement, bentonite, and water. The materials present in the mixture were characterized by another study (Azadi et al., 2017). The density of the waste matrix was derived from the drum weight measurements (Vaidotas, 2013).

For the drum lining a standardized material “Steel, Medium Carbon (328)” was used as the carbon amount closely matched with a previously studied storage drum composition (Li et al., 2019). The concrete container and surrounding air were composed of standardized materials, “Portland Cement Concrete” and “Dry Air, Near Sea Level”, respectively (PNNL, 2021).

The model setup with five different overpack materials were compared against each other. The first material, cement paste, served as a baseline, and is currently used for grouting the waste drums in place. The chemical composition of this material was taken from the literature (Tsardaka et al., 2023). Oil-shale ash and basalt-boron fiber concrete were prepared experimentally. After testing, the material chemical composition was analyzed using an XRF-method and LOI was corrected by increasing the content of hydrogen and carbon.

Each concrete contained a different amount of oil-shale ash and basalt-boron fibers. More detailed information about BB fibers used in fiber concrete fabrication can be found in the literature (Tohver et al., 2024; Romanenko et al., 2019). The selection of four concretes also

included one, which did not contain any oil-shale ash, but did include the fibers. The weight-fraction based recipes for overpack materials can be found in Table 2 and elemental composition in Table 3.

Table 2: The concrete recipes of the modeled cement paste and four concrete mixes experimentally created during this study. The quantities are given in weight fractions.

Ingredients / Recipes	Cement Paste	E3-0	E3-1	G3-1	G3-3
Schwenk Eco cement CEM II A-LL 42.5 N	7.143E-01	1.298E-01	1.241E-01	1.282E-01	1.266E-01
Oil shale ash (OSA)	0	0	7.020E-03	6.391E-03	1.901E-02
Water	2.857E-01	7.659E-02	7.020E-02	7.148E-02	7.057E-02
Dolomite 4-8 mm	0	4.451E-01	4.477E-01	4.398E-01	4.342E-01
Sand 0.3-2.5 mm	0	2.570E-01	2.585E-01	2.540E-01	2.507E-01
Sand 0-1.0 mm	0	4.851E-02	4.880E-02	4.794E-02	4.733E-02
Dolomite flour	0	3.489E-02	3.510E-02	3.448E-02	3.404E-02
Plasticizer	0	4.766E-03	5.051E-03	4.205E-03	4.151E-03
Basalt-boron fibers (BBF)	0	3.404E-03	3.424E-03	1.346E-02	1.328E-02

Fiber concrete sample-cubes were fabricated with different concentrations of short BBFs. The samples were created using typical concrete ingredients such as: Schwenk Eco cement CEM II A-LL 42.5 N, oils shale ash (OSA, Estonia), Water, Dolomite gravels 4-8 mm, Sand 0.3-2.5 mm (Saulkalne, Latvia), Sand 0-1.0 mm (Saulkalne, Latvia), Dolomite flour, Plasticizer (Sika D190) and BBFs. The process of making the concrete cubes can be seen in Fig. 2. The concrete components without BBFs were mixed in a separate bucket. A layer of fresh concrete, 3-4 cm thick, was created in a separate container. It was covered with fibers and mixed. Then the next layer of concrete was added, covered again with fibers and then mixed. At the beginning with combs, then with a mixer. In this way, step by step, the necessary amount of fibers were mixed with concrete. After that, fresh fiber concrete was

poured into the cube molds with dimensions of 100x100x100 mm. The moulds were vibrated on a vibrating table for a couple of minutes. After 2-3 days, the cubes were removed from the molds and placed in a bath with a constant temperature of water 20±2 °C. After 28 days samples were ready for measurement.

a) b) c) d)

Figure 2: a) BB short fibers; b) concrete layer with fibers on its surface; c) mixing; d) fresh fiberconcrete cubes in moulds on the vibrating table.

E3-0 and E3-1 are fiber concretes with the same BB fibers concentration. The concretes were manufactured using 6mm long fibers and had lower fiber concentration when compared to the rest of the samples. Concrete E3-0 does not contain OSA. For the E3-1 mix, 5.4% of the cement was replaced with OSA. Since one of the goals was to have samples with similar rheological parameters, a small deviation in other ingredient fractions was introduced during the manufacturing process (controlled by Abrams c.).

G3-1 and G3-3 are fiber concrete samples with the equal BBF concentration but are characterized by a higher concentration than samples E3-0 and E3-1. Fibers were 24mm long (see Fig. 2.a). The amount (absolute value) of cement (CEM II A-LL 42.5 N) in G3-1 and G3-3 was the same as in the samples E3-0. For the sample G3-1, 5% (compared to the cement's absolute weight) of OSA was added to the mix, and 15% (compared to the cement's absolute weight) of OSA to sample G3-3. The densities and elemental weight fractions are displayed in Table 3.

Table 3: Densities (g/cm^3) and elemental weight fractions of studied overpack concrete.

	Cement Paste	E3-0	E3-1	G3-1	G3-3
Densities (g/cm^3)					
ρ	1.934	2.405	2.419	2.413	2.403
Elemental weight fractions					
Si	5.907E-02	1.237E-01	1.261E-01	1.265E-01	1.289E-01
Al	1.533E-02	1.220E-02	1.227E-02	1.289E-02	1.297E-02
Fe	2.744E-02	1.001E-02	9.869E-03	1.065E-02	1.060E-02
Ti	1.091E-03	4.630E-04	4.606E-04	5.279E-04	5.295E-04
Ca	3.090E-01	1.830E-01	1.822E-01	1.822E-01	1.815E-01
Mg	1.050E-02	6.295E-02	6.340E-02	6.271E-02	6.221E-02
Na	5.050E-04	2.252E-03	2.292E-03	2.384E-03	2.410E-03
K	6.168E-03	6.598E-03	6.665E-03	6.712E-03	6.777E-03
Mn	3.599E-04	4.961E-04	4.970E-04	5.036E-04	4.994E-04
S	3.887E-03	1.055E-03	1.036E-03	1.052E-03	1.054E-03
P	3.057E-04	1.261E-04	1.254E-04	1.311E-04	1.316E-04
V	3.512E-05	8.499E-06	1.015E-05	1.442E-05	1.770E-05
Cr	3.723E-05	1.526E-05	1.516E-05	1.521E-05	1.527E-05
Co	2.107E-05	1.642E-05	1.633E-05	1.645E-05	1.624E-05
Ni	0.000E+00	4.900E-08	1.571E-07	2.918E-07	4.832E-07
Cu	3.442E-05	6.332E-06	6.061E-06	6.491E-06	6.408E-06
Zn	1.166E-04	2.510E-05	2.420E-05	2.586E-05	2.553E-05
Ga	4.917E-06	2.117E-06	2.086E-06	2.237E-06	2.209E-06
Ge	0.000E+00	1.339E-06	1.347E-06	1.323E-06	1.306E-06
As	0.000E+00	0.000E+00	0.000E+00	0.000E+00	0.000E+00
Se	0.000E+00	0.000E+00	0.000E+00	0.000E+00	0.000E+00
Br	2.810E-06	9.346E-06	9.377E-06	9.236E-06	9.118E-06
Rb	1.967E-05	1.975E-05	1.969E-05	2.011E-05	1.985E-05
Sr	4.446E-04	1.566E-04	1.549E-04	1.588E-04	1.592E-04
Y	4.917E-06	1.046E-06	1.008E-06	1.486E-06	1.467E-06
Zr	0.000E+00	8.441E-06	8.492E-06	8.573E-06	8.464E-06
Nb	3.512E-06	6.381E-07	6.104E-07	6.306E-07	6.226E-07

Mo	3.091E-05	5.615E-06	5.371E-06	5.549E-06	5.479E-06
Ba	8.921E-05	8.443E-05	8.414E-05	8.589E-05	8.480E-05
Sm	4.025E-04	7.313E-05	6.995E-05	7.227E-05	7.135E-05
Pb	4.285E-05	1.023E-05	9.910E-06	1.044E-05	1.031E-05
O	5.212E-01	5.237E-01	5.219E-01	5.212E-01	5.207E-01
H	3.280E-02	1.029E-02	9.606E-03	9.641E-03	9.524E-03
C	1.102E-02	6.263E-02	6.299E-02	6.197E-02	6.134E-02
Cl	0.000E+00	3.413E-07	3.433E-07	1.349E-06	1.332E-06
B	0.000E+00	1.019E-04	1.025E-04	4.029E-04	3.977E-04

Although the content of oil-shale ash and basalt-boron varied, the density of each concrete was relatively constant, around 2.4 g/cm3. The density of OSA-BBF concrete was higher than the cement paste (1.9 g/cm3) and standardized Portland concrete (2.3 g/cm3).

2.3. Radiation source description

To properly evaluate the effective dose, the nuclide composition of the modeled waste must be known. For this purpose, prior measurements and analysis of INPP low- and intermediate-level liquid waste were used (Vaidotas, 2013). These measurements included the average activity of primary nuclides (Cs-137, Co–60) which were used to assess the composition of the rest of the waste. A full gamma-spectrum of evaluated radionuclides was then created, but only radionuclides which contributed with more than 0.1% of the emissions were used in final dose estimations. The data necessary to construct the gamma-spectrum was taken from the LNHB public nuclide database (*Mini Table De Radionucléides,* 2015).

The only radionuclides that satisfied the above-mentioned criteria were Cs-137, Co-60, Cs-134, and Mn-54. Since these radionuclides cover a large range of half-lives (30 years, 5 years, 2 years, and 312 days respectively), it was decided to model the decay of these nuclides to calculate the effective dose in time. Oftentimes, the disposal of liquid waste does not take place right after the generation of the waste, but up to 20 years and potentially even further in the future. During this time, the liquid waste is kept in large storage tanks.

The estimated radionuclide activities over 20 years (since the measurement) are described in Table 4.

Table 4: Activities (Bq) of radionuclides present in the waste matrix over 20 years.

	Co-60	**Cs-137**	**Cs-134**	**Mn-54**
0 years	1.76E+09	2.63E+09	9.32E+07	2.17E+07
5 years	9.12E+08	2.34E+09	1.74E+07	3.76E+05
10 years	4.73E+08	2.09E+09	3.25E+06	6.51E+03
15 years	2.45E+08	1.86E+09	6.06E+05	1.13E+02
20 years	1.27E+08	1.66E+09	1.13E+05	1.96E+00

At the start, the activities of Co-60 and Cs-137 are quite similar, but due to Co-60 short half-life, the gap between these two radionuclides quickly grows with time. It must be noted that Co-60 is responsible for more than twice the amount of emissions per decay with average emission energy being close to double as well, which is why Co-60 can be more dangerous from gamma-radiation point of view. Cs-134 and Mn-54 have non-negligible activity at measurement, but Mn-54 decays rapidly (5 years is enough to reduce the activity by almost 2 orders of magnitude) and Cs-134 is quick to follow.

A gamma-emission spectrum was created for each of the radionuclide and modeled using a discrete spectra approach. The source was modeled uniformly throughout the waste material with isotropic emissions. Each radionuclide-overpack material combination was assessed separately to reduce the total amount of simulations necessary. One positive side to this approach was the flexibility of the calculated results (dose rate per unit activity, henceforth dose coefficient), which made it possible to assess the dose rate for an arbitrary combination of the above-mentioned four radionuclides.

2.4. Scoring and tallies

The dose coefficients were calculated by assessing the flux near the concrete container sides. For this purpose, a 20 cm x 20 cm x 10 cm cuboid cell of air was placed against the short and long side of the container. The cells' placement corresponded with the position of drums in the container. Thus, the cell detectors were placed such that they covered the air region closest to the waste. The thickness of the cell detectors was taken to be 10 cm, which corresponds to the estimation of the regulated dose limit criteria (2 mSv/h at the surface of the container) and the average dimensions of the measuring apparatus. The location of the cells is shown in Fig. 3.

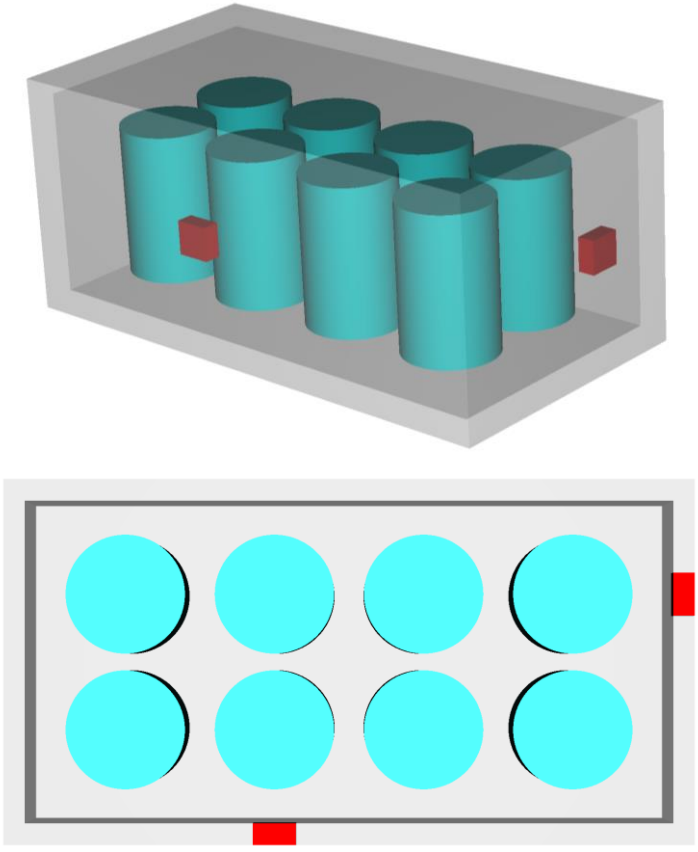

Figure 3: Top and isometric view of detector locations for the Framatome-ANP waste package geometry visualized using EGSVIEW. Only the waste drums and surrounding air shown.

In addition to the air detector cells, a general mesh tally was overlaid across the whole geometry with cubic voxels of length 2.5 cm. This provided a better understanding of how the dose develops across multiple material boundaries and outside the concrete container.

The flux was evaluated for 25 different energy groups, from 0.01 keV to 1.5 MeV in a geometrical progression. This was done to account for the combined effect of direct and secondary scattered radiation on the dose rate. The evaluated energy flux was converted to dose using flux to effective dose coefficients. To use the latest coefficients published by the ICRP (IAEA, 2012), the dose to flux coefficients were linearly interpolated to match the average energy of each flux energy group. Out of all the phantom configurations, the coefficients for the antero-posterior (AP) setup were used as it offers the most conservative evaluation for particle energies below 6 MeV.

3. Results and discussion

The analysis of OSA-BBF concrete's gamma-radiation shielding properties is divided into three sections. First, the output of each code is compared to verify if the model setup was correct and whether any bias could be identified. This is done by focusing on each nuclide and looking at their contribution separately. The second section focuses on the total external effective dose in time and the last section analyzes the dose map view to characterize the internal and external effective dose distribution.

3.1. Nuclide-specific effective dose rate coefficients of the air surrounding the container

The coefficients for effective dose rates per nuclide (in μSv GBq^{-1} h^{-1}) enable the calculation of effective doses within the same geometry, considering varying activity levels in the radiation source. Serpent (Leppänen et al., 2013), SCALE (Wieselquist et al., 2020), MCNP (Werner, 2017), EGSnrc (Kawrakow et al., 2021) and OpenMC (Romano et al., 2015) were used to calculate the flux contribution from Co-60, Cs-137, Cs-134, and Mn-54 separately. While this approach comes with an extra computational cost when assessing a source with a specific radionuclide composition, it offers additional flexibility and can be less resource-intensive when the activity of the source changes over time and there is a need to assess many different source configurations. The results are shown in Figs. 4 and 5 for the long side and short side respectively and reported at 2 standard deviations (Monte Carlo statistical error). The results shown in Fig. 4 are also presented in Table 5.

Table 5: Dose coefficients (μSv GBq^{-1} h^{-1}) describing the long side of the waste container for modeled nuclide and material combinations.

	Co-60	**Cs-137**	**Cs-134**	**Mn-54**	**Co-60**	**Cs-137**	**Cs-134**	**Mn-54**
Code	**Cement**				**G3-1**			
SCALE	11.304	1.417	4.120	2.662	10.049	1.227	3.590	2.346
EGSnrc	11.211	1.406	4.030	2.673	10.086	1.230	3.569	2.310

OpenMC	11.326	1.415	4.129	2.678	10.050	1.224	3.590	2.340
Serpent	11.281	1.398	4.110	2.675	10.012	1.223	3.563	2.335
MCNP	11.249	1.413	4.104	2.672	9.973	1.228	3.565	2.332
	E3-0				**G3-3**			
SCALE	10.000	1.232	3.603	2.342	10.025	1.240	3.603	2.345
EGSnrc	10.055	1.218	3.547	2.357	10.015	1.240	3.572	2.328
OpenMC	10.070	1.227	3.598	2.345	10.086	1.229	3.605	2.348
Serpent	10.029	1.219	3.568	2.338	10.039	1.229	3.584	2.334
MCNP	9.991	1.231	3.572	2.337	10.008	1.233	3.580	2.340
	E3-1							
SCALE	10.010	1.228	3.594	2.348				
EGSnrc	10.008	1.229	3.573	2.312				
OpenMC	10.035	1.223	3.588	2.336				
Serpent	10.016	1.222	3.573	2.338				
MCNP	9.965	1.225	3.557	2.328				

Out of the investigated radionuclides, the decay of Co-60 results in the highest dose rate near the surface of the container. This can be explained by three factors. First, each decay of Co-60 results on average the emission of 1.998 high energy gamma particles, compared to 0.850 for Cs-137 and 1.0 for Mn-54. Even if the particle count per emission is higher, such as Cs-134 (2.185), the dose coefficient is lower than Co-60's since the average energy of emitted particles is not as much. Co-60 emits 1.17 MeV and 1.33 MeV particles while the most probable emissions for Cs-134 are at 0.60 MeV and 0.80 MeV. In fact, the emission energy for Cs-137 is 0.66 MeV and for Mn-54 it is 0.83 MeV, making Co-60 emit the highest amount of energy per decay out of the investigated radionuclides.

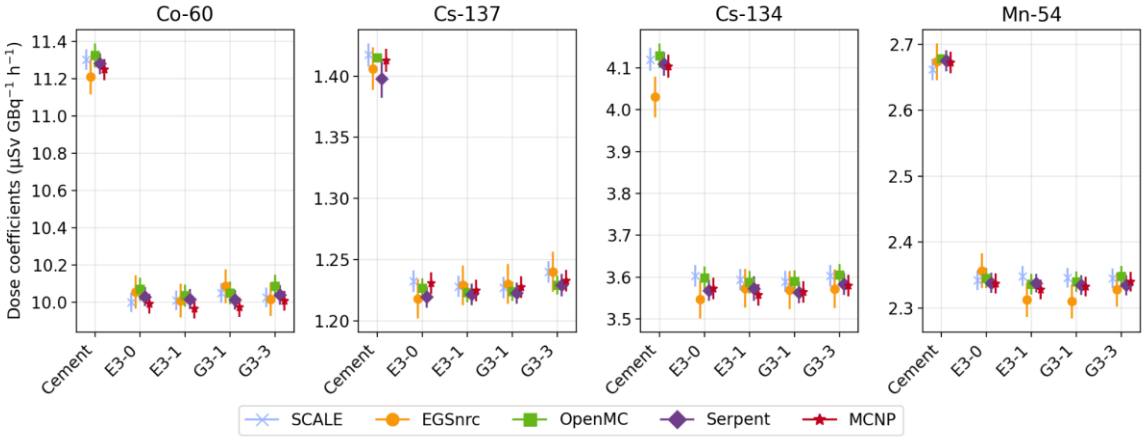

Figure 4: Nuclide- and material-specific effective dose rate coefficient estimations for the detector at the long side of the container using SCALE, EGSnrc, OpenMC, Serpent, and MCNP.

Radionuclides with high emission energy can influence the external dose more due to the greater penetration capability and larger flux to dose conversion factors. Dose conversion factors are governed by a mostly linear function (region of 100 keV to 1.5 MeV), meaning that particle flux with higher average energy results in a higher dose. The same trends were observed for both sides of the container, making Co-60 the highest contributor per activity, followed by Cs-134, Mn-54 and then Cs-137.

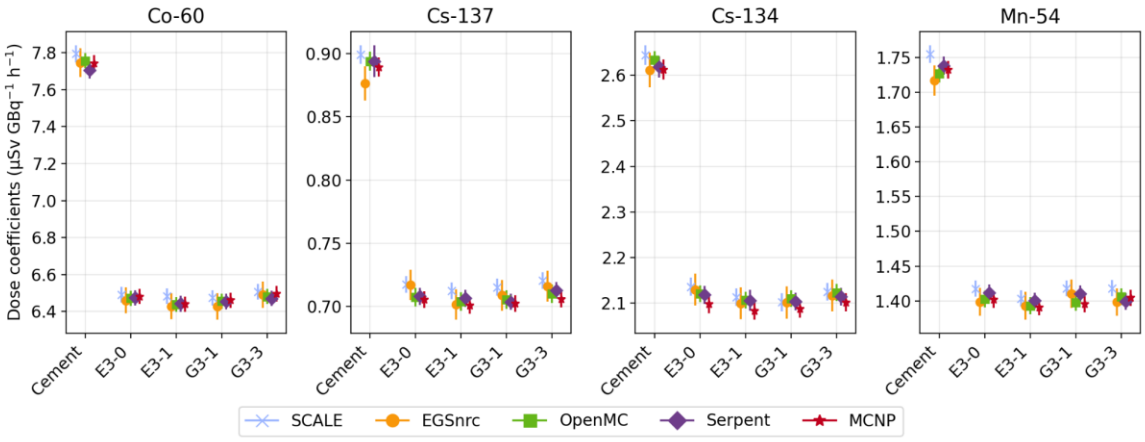

Figure 5: Nuclide- and material-specific effective dose rate coefficient estimations for the detector at the short side of the container using SCALE, EGSnrc, OpenMC, Serpent, and MCNP.

The choice of material had a significant influence on the dose rate coefficient. The basic cement paste showed higher coefficients compared to the prepared OSA-BBF concrete. This can be likely explained by the density difference between the materials (1.9 vs 2.4 g/cm3). The OSA-BBF concrete recipes demonstrated very similar photon attenuation properties. Any change in the photon attenuation properties can be attributed to differences in elemental composition and bulk density. The studied concretes had different levels of oil shale ash and basalt boron fiber content.

The ash used to make the concrete contains 48% percent oxygen, 31% silicon, 13% calcium, 2% magnesium and carbon. These five main elements make up more than 95% of the elemental composition of the additive. In a similar vein, the basalt boron additive is composed of 48% oxygen, 23% silicon, 7% aluminum, 7% iron, 6% calcium, 3% magnesium and boron, making up over 96% of the elemental composition. While the basalt boron additive has a larger variety of elements, the composition is still made up of lighter elements, which have very similar total attenuation factors (Fig. 6) in the range of 200 keV to 5 MeV, where all of the waste source emissions can be found. The previously named elements were observed to be responsible for the largest differences in the elemental composition of different concretes.

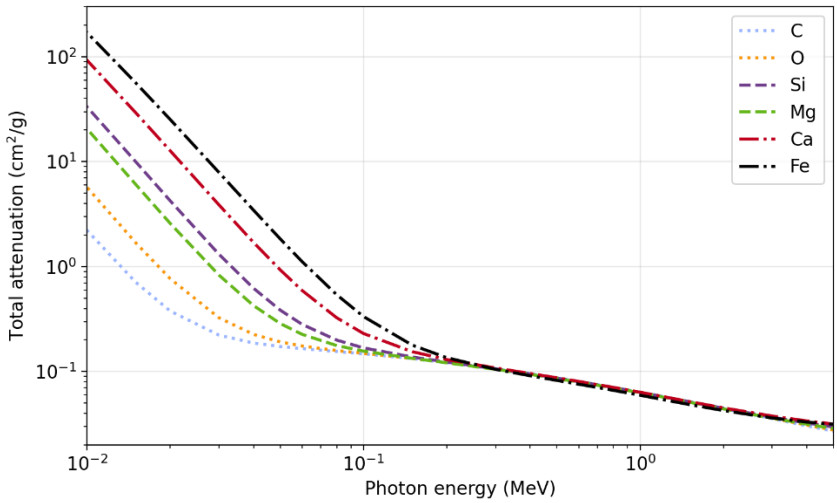

Figure 6: Total attenuation factors describing the main elements of the additives. The attenuation factors were retrieved from NIST's XCOM database (Berger, et al., 2010).

Therefore, the question is not on how the elemental composition changes, but rather the bulk density. Bulk density depends on more factors than just the elemental composition, which is one of the reasons why the concrete samples were prepared experimentally. Given the varying content of additives in the concrete analyzed in this study, but similar densities, it can be concluded that the additives can be added without having to compromise on the bulk density of the concrete.

All codes were in agreement with each other and had overlapping uncertainties (reported at two standard deviations) for almost all material and radionuclide combinations. One outlier was EGSnrc (Cement and Cs-134 combination), but EGS is also accompanied by the largest uncertainties. One potential reason is the fact that EGSnrc is code specially focused on low energy emissions and the improved algorithms might be indicative of a lower dose-rate for low-energy emission (Cs-134 emission spectrum) and low-density concrete combination. In any case, the error between EGSnrc and the rest of the codes is relatively small (less than 3%) for even the largest discrepancy.

3.2. Effective dose rate in the air surrounding the waste container

Since there were only marginal differences in the output of the investigated codes, with overlapping uncertainties, the results shown in this section have been merged by calculating the arithmetic mean. By using the initial activities described in Table 4, the total dose contribution of each radionuclide was calculated at the surface of the long and short side of the container. The results are shown in Fig. 7.

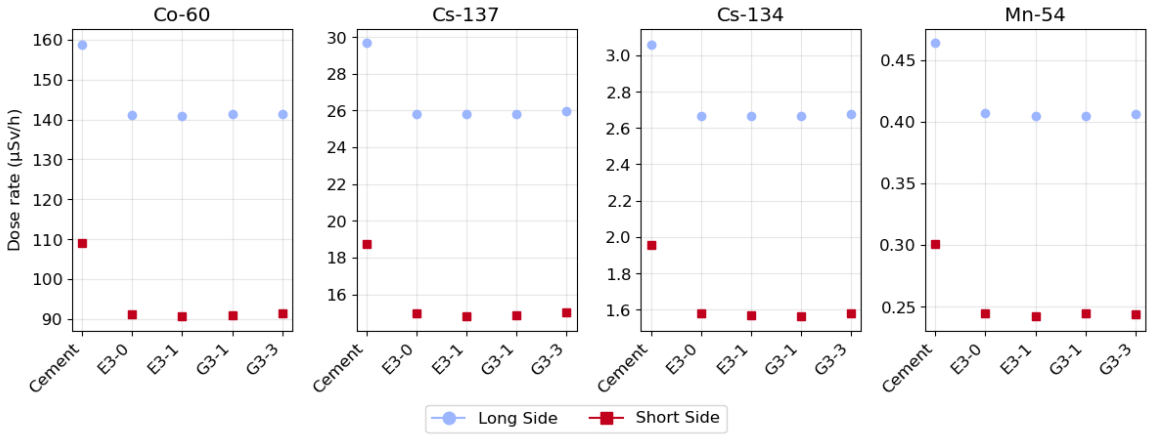

Figure 7: Nuclide- and material-specific averaged effective dose rates (before decay, at time 0, Table 4) for both cell detectors.

The largest contributor to external dose was Co-60, which was similar to the dose rate coefficient order of contribution. However, the second place was not Cs-134, but Cs-137. The activity of Cs-137 is roughly an order of magnitude higher than its neighboring isotope Cs-134, which was also reflected in the dose rate estimation. Out of all the radionuclides, Mn-54 contributed with a dose rate that was lower by another order of magnitude, making up more than 0.1% but less than 1% of the total dose contribution.

Next off, the contribution of each radionuclide was summed up to calculate the total dose rate in air at the surface of the container. The summed dose rates were calculated over a period of 20 years and are visualized in Fig. 8.

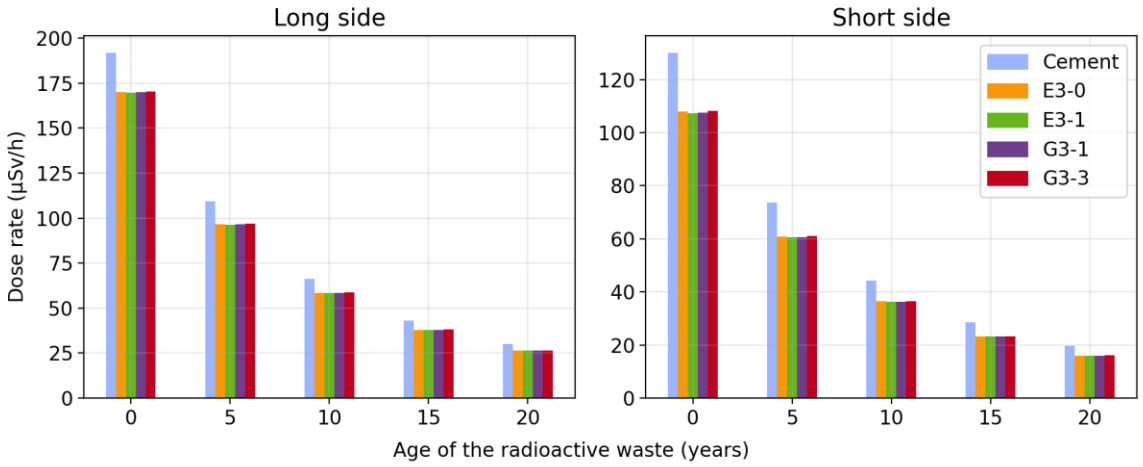

Figure 8: Material-specific total averaged effective dose rates for both cell detectors in time.

The radioactive waste comprises radionuclides with diverse half-lives, ranging from 30 years (Cs-137) to less than a year (Mn-54). Each radionuclide's activity within the waste mixture exhibits a varying rate of change, as outlined in Table 4. Notably, within the first 5 years, the total dose rate experiences a more pronounced decrease due to the substantial alteration in the contribution of shorter-lived radionuclides like Mn-54 and Cs-134, changing by over tenfold.

Initially for cement paste, the total dose rate at the long side was 192 μSv/h and at the short side was 130 μSv/h. The total average dose rate for the OSA-BBF concrete at the long side was 170.1 ± 0.4 μSv/h and 107.8 ± 0.6 μSv/h for the short side. The error in OSA-BBF concrete dose assessment is reported at 2 standard deviations (Monte Carlo statistical error). The difference between cement paste and OSA-BBF concrete was 12.8% for the long side and 20.7% for the short side.

The difference between the two sides slightly increased over time with 13.0%, 21.1% at 5 years, 13.3%, 21.7% at 10 years, 13.6%, 22.5% at 15 years, and 13.9%, 23.2% at 20 years for the long and short side respectively. Thus, the average rate of change of the difference between the two types of concrete was 0.3% and 0.6% for each of the observed five year periods.

The dose rate itself changed quite a bit. After 20 years, for cement paste, the total dose

rate at the long side was 30 μSv/h and at the short side 20 μSv/h, meaning that the dose rate from the decayed waste had a 6.5 times lower effect on the external dose rate than at the beginning. The total average dose rate for the OSA-BBF concrete after 20 years was 26.50 ± 0.02 μSv/h and 15.99 ± 0.01 μSv/h at the long and short side, showing similar differences as the cement paste.

The calculated total dose rates at the surface of the container do not exceed the limit values set at the Ignalina Nuclear Power Plant in any scenario. Given the relatively small dose rates, there is a significant safety margin, which might make it possible to start waste management of liquid wastes even sooner with only a small negative effect on the worker doses. By using OSA-BBF concrete, the radiation dose near the vicinity of the packages is expected to be lower than materials currently in use. Since the dose rate was not notably sensitive to the OSA and BBF content, these additives can be added without limit from radiation protection point of view.

3.3. Mapping the effective dose rate of the container

The regulated dose limits for radioactive waste containers are located at the surface or at a distance of 0.1 m from the surface of the containers. A mesh of 2.5 cm voxels overlaid the entire geometry with 25 different energy bins. The energy distribution in each voxel could be calculated into a local effective dose rate estimation. The modeling was done using OpenMC and G3-3 concrete, which contained the largest amount of oil shale ash.

Analyzing the effective dose rate distribution showed that expectedly, the highest dose rate is located at the center of the waste drums. A slice through the center of the container and through the center of the first row of waste drums is shown in Fig. 9. The borders of the geometry are overlaid on top of the dose rate map. The maximum dose rate at the center is 8.36 mSv/h and the minimum dose rate at the corner of the geometry is 10 μSv/h.

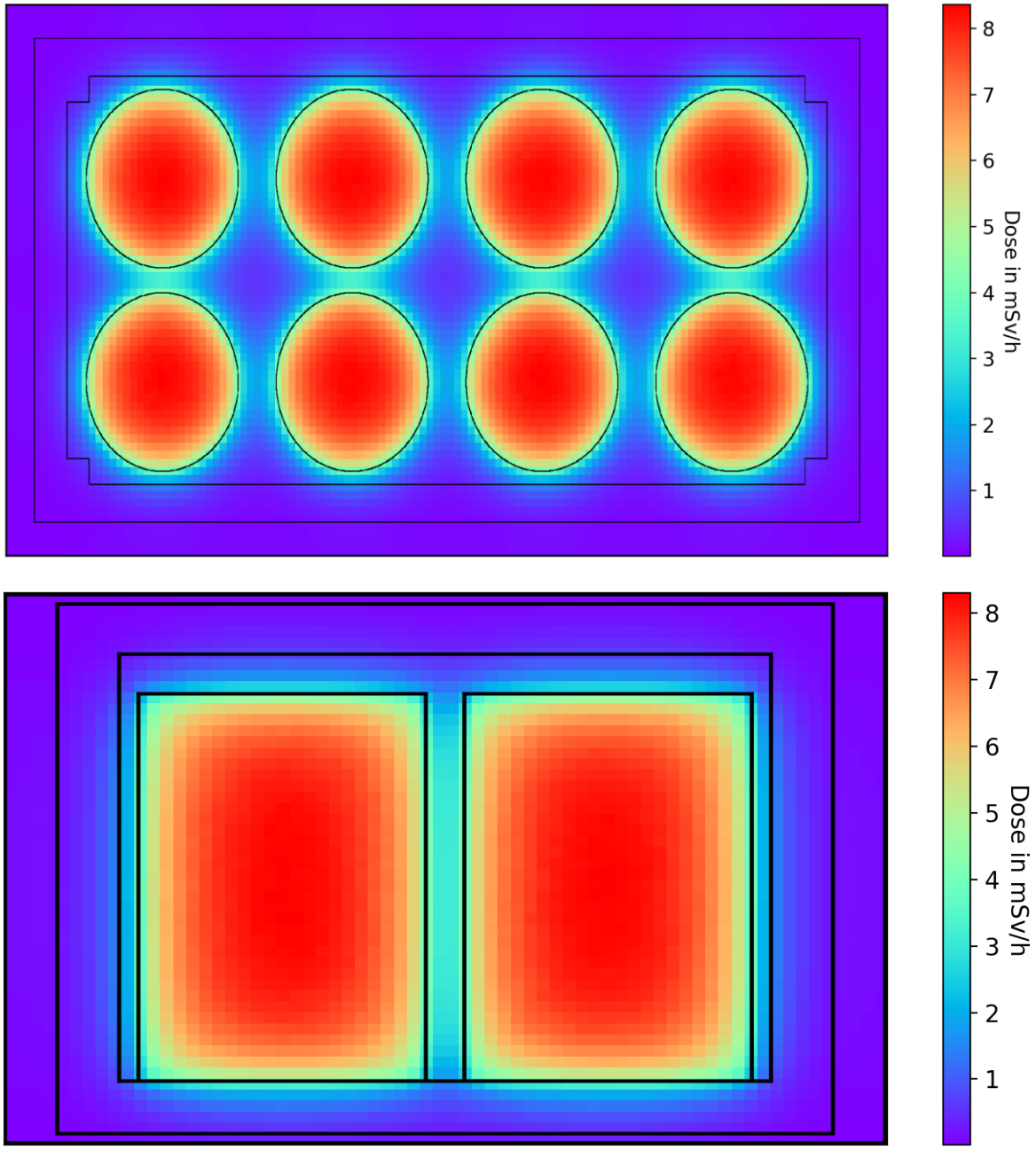

Figure 9: Total effective dose rate (before decay, at time 0, Table 4) distribution top- and side-view for the waste container using G3-3 concrete.

Near the vicinity of the waste drums, the dose rate was roughly 4 mSv/h. In the document that characterized the isotopic composition of the waste, average dose rates of 1.6 mSv/h and

maximum dose rates of 4 mSv/h were measured 0.1 m away from the surface of the drums. These values coincide, but one-to-one comparison cannot be made as in this geometry, the drums are surrounded by the overpack, and not air. The surrounding overpack reduces the dose rate much more rapidly than the same thickness of air.

A relatively large region of high dose rates was formed in the center of the container where the waste drums were close. The average dose rate in that region was around 3 mSv/h. This region would likely see the biggest impact from any radiolysis effects, outside of the waste drum surfaces. If any future studies are done on the sensitivity of the OSA-BBF concrete to radiation damage, this region might be of special interest.

To understand how OSA-BBF concretes affect the dose distribution generally, the side-view dose map from the cement paste was compared to the innovative concrete. Since the dose values varied by more than an order of magnitude, the difference in dose rates was expressed using a linear scale and (C/O - 1) * 100%, where C is the cement paste dose rate, and O is the dose rate for OSA-BBF concrete. The results are visualized in Fig. 10.

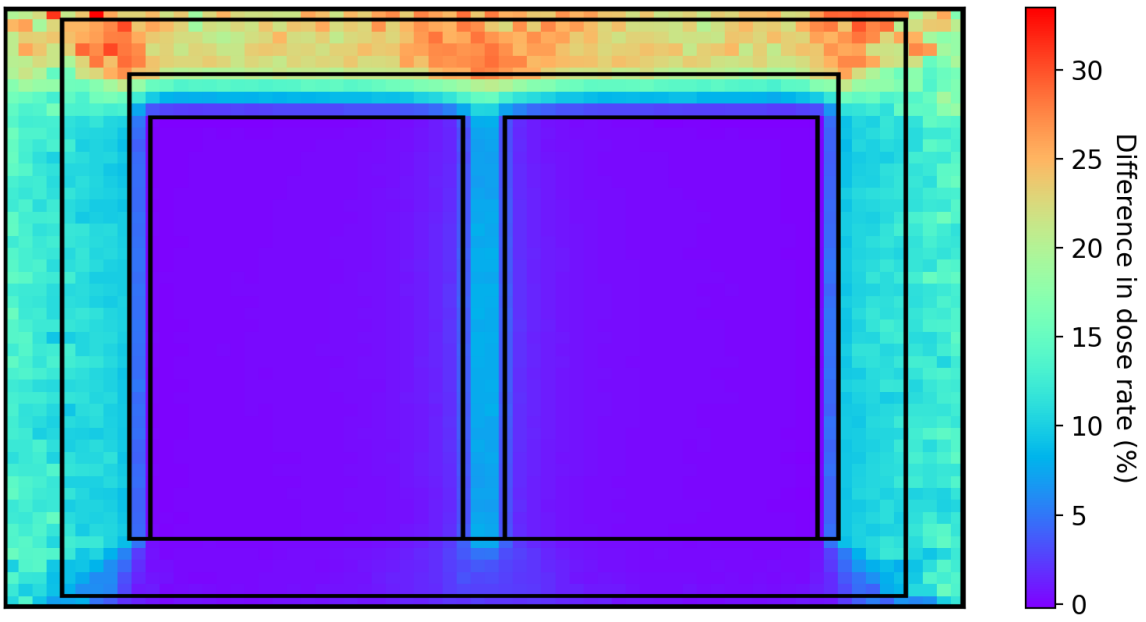

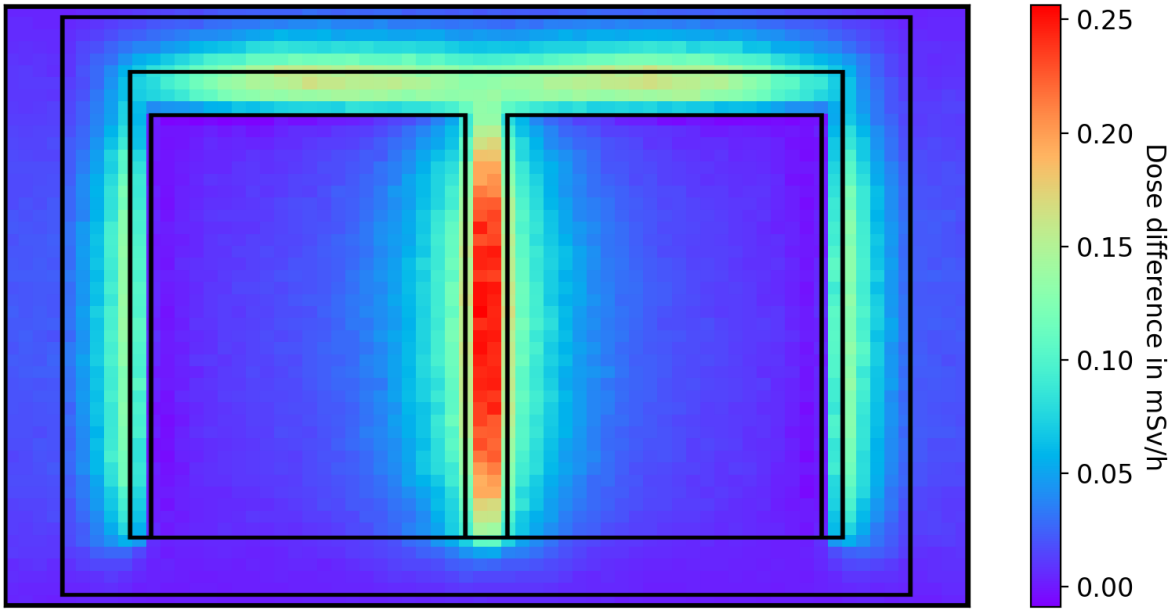

Figure 10: Total effective dose rate (before decay, at time 0, Table 4) distribution difference in the waste container using cement paste and G3-3 concrete.

The region with the largest absolute difference of 0.25 mSv/h was observed in the previously described section between the drums. However, when the ratio of change was calculated, this region showed only around 10% of change. The largest relative change in the dose rate took place on top of the drums. This is understandable, as the thickest layer of overpack between the drums and the container is on top of the drums. The change in this region reached upwards of 30%, between 0.10 and 0.20 mSv/h. However, this decrease in the dose rate will not have a large impact on the radiation shielding aspects as the Framatome ANP waste containers are generally stacked on top of each other, thereby shielding the top part of most containers.

Finally, the dose rate distribution in the air outside of the container was analyzed as well. Each side of the container was surrounded by 10 cm of air. Since the mesh voxel size was 2.5 cm, it was possible to sum together 4 outermost mesh layers and calculate the average to represent the 10 cm thick air layer surrounding the package. These dose rate distribution maps are shown in Fig. 11.

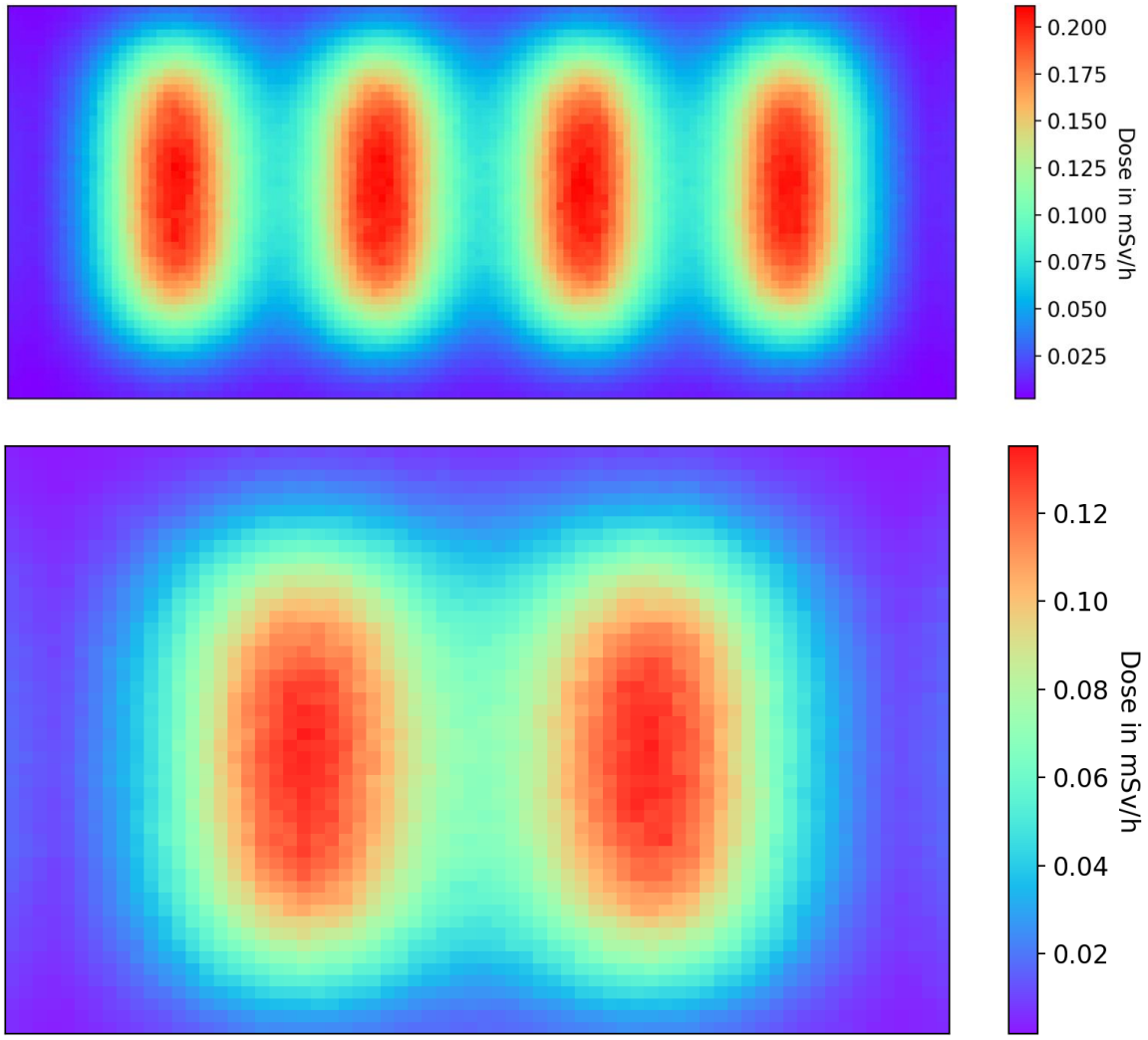

Figure 11: Total effective dose rate distribution side-views (long side and short side) in the 10 cm layer of air around the container.

These distributions show that while the shorter side is better shielded and thus results in lower dose rates, the minimum dose rate locations of both sides are quite similar, around 0.01 mSv/h, and are located at the far corners of the container. The general region of high dose follows the shape of the waste drums accurately, with the short side having 2 local maxima and long side 4 local maxima. The average dose rate in air, up to 10 cm away from

the container, is 52 μSv/h and 83 μSv/h at the short and long side respectively.

4. Conclusions

The main goal of the study was to investigate whether the inclusion of oil shale ash and basalt-boron fibers would deteriorate the radiation shielding properties enough to make it unsuitable for waste package applications. For this purpose, model geometry of the Framatome-ANP waste container was created using OpenMC, EGSnrc, SCALE, MCNP, and Serpent. The geometry was investigated by analyzing the low- and intermediate-level waste from the Ignalina Nuclear Power Plant and modeling waste gamma-emissions. 4 different OSA-BBF concrete recipes were prepared and compared against a standard cement paste recipe.

The container surface dose estimations showed excellent agreement between all the codes. The container surface dose remained well within limit values specified by safety standards, indicating significant safety margins and potential for earlier management of liquid waste without substantial impact on worker doses. Dose rate distribution mapping within container geometries demonstrated expected trends, with higher rates near waste drums, notably impacting regions closer to waste drum surfaces, potentially warranting future studies on OSA-BBF concrete's sensitivity to radiation damage in these areas. Comparison between OSA-BBF concrete and traditional cement paste revealed differences in dose rates, emphasizing the potential for OSA-BBF concrete to lower radiation doses near waste packages due to its shielding properties. The analysis extended to dose rate distributions outside the container, showcasing variations consistent with waste drum shapes and placement.

In summary, this investigation underscores the promising radiation shielding capabilities of OSA-BBF concrete, suggesting its potential for effective use in radioactive waste management practices, offering superior shielding properties compared to conventional materials. The study's findings are especially promising for regions with abundant oil shale

resources, such as the Baltics, and can be potentially applied in the waste management taking currently in the Ignalina Nuclear Power Plant (Lithuania), or future decommissioning of the Paldiski Nuclear Site (Estonia), which contains only low- and intermediate-level waste.

Funding

This work was carried out within the "Innovation in concrete design for hazardous waste management applications" (ICONDE) project, EEA-RESEARCH-165, financially supported by the European Economic Area (EEA) Grants of Iceland, Liechtenstein, and Norway.

Credit Author Statement

Hando Tohver – Methodology, Software, Validation, Formal analysis, Writing - Original Draft, Visualization

Andrius Slavickas – Methodology, Software, Validation, Writing - Review & Editing

Maryna Holiuk – Methodology, Software, Validation, Writing - Review & Editing

Andrejs Krasņikovs – Resources, Writing - Review & Editing

Riho Mõtlep – Resources, Writing - Review & Editing

Iveta Nováková - Resources

Egidijus Babilas - Writing - Review & Editing, Supervision

Volodymyr Gulik – Conceptualization, Methodology, Supervision

References

Azadi, M. R., Taghichian, A., & Taheri, A. (2017). Optimization of cement-based grouts using chemical additives. *Journal of Rock Mechanics and Geotechnical Engineering*, *9*(4). https://doi.org/10.1016/j.jrmge.2016.11.013

Berger, M. J., Hubbell, J. H., Seltzer, S. M., Chang, J., Coursey, J. S., Sukumar, R., Zucker, D. S., Olsen, K. (2010). XCOM: Photon Cross Sections Database.

doi:https://dx.doi.org/10.18434/T48G6X

Han, D., Kim, W., Lee, S., Kim, H., & Romero, P. (2018). Assessment of gamma radiation shielding properties of concrete containers containing recycled coarse aggregates. *Construction and Building Materials, 163*. https://doi.org/10.1016/j.conbuildmat.2017.12.078

IAEA. (2006). *IAEA-TECDOC-1515: Development of Specifications for Radioactive Waste Packages*. International Atomic Energy Agency.

IAEA. (2012). *ICRP Publication 116: Conversion Coefficients for Radiological Protection Quantities for External Radiation Exposures*. SAGE Publications.

Kawrakow, I., Rogers, D. W. O., Mainegra-Hing, E., Tessier, F., Townson, R. W., & Walters, B. R. B. (2021). *EGSnrc toolkit for Monte Carlo simulation of ionizing radiation transport*. National Research Council of Canada. https://doi.org/10.4224/40001303

Leben, K., Mõtlep, R., Paaver, P., Konist, A., Pihu, T., Paiste, P., Heinmaa, I., Nurk, G., Anthony, E. J., & Kirsimäe, K. (2019). Long-term mineral transformation of Ca-rich oil shale ash waste. *Science of The Total Environment, 658*. https://doi.org/10.1016/j.scitotenv.2018.12.326

Leppänen, J., Pusa, M., Viitanen, T., Valtavirta, V., & Kaltiaisenaho, T. (2013). The Serpent Monte Carlo code: Status, development and applications in 2013. *Annals of Nuclear Energy*, 142-150. https://doi.org/10.1016/j.anucene.2014.08.024

Li, J., Chen, L., & Wang, J. (2021). Solidification of radioactive wastes by cement-based materials. *Progress in Nuclear Energy, 141*. https://doi.org/10.1016/j.pnucene.2021.103957

Li, W., Liu, X., Li, M., Huang, Y., & Fang, S. (2019). Multilayer Shielding Design for Intermediate Radioactive Waste Storage Drums: A Comparative Study between FLUKA and QAD-CGA. *Science and Technology of Nuclear Installations, 2019*. https://doi.org/10.1155/2019/8186798

Mini table de radionucléides 2015. (2015). EDP Sciences.

Nabil, I. M., El-Samrah, M. G., Omar, A., Tawfic, A. F., & El Sayed, A. F. (2023). Experimental, analytical, and simulation studies of modified concrete mix for radiation shielding in a mixed radiation field. *Scientific Reports, 13*. https://doi.org/10.1038/s41598-023-44978-8

Nuclear Waste Services. (2022). *Specification for Waste Packages Containing Low Heat Generating Waste Part D - Container Specific Requirements*. Nuclear Decommissioning Authority.

Ochs, M., Mallants, D., & Wang, L. (2015). *Radionuclide and Metal Sorption on Cement and Concrete*. Springer International Publishing.

OECD/NEA. (2012). *Cementitious Materials in Safety Cases for Geological Repositories for*

Radioactive Waste: Role, Evolution and Interactions (A workshop organised by the OECD/NEA Integration Group in the Safety Case and hosted by ONDRAF/NIRAS ed.). OECD/NEA.

PNNL. (2021). *Data Mining Analysis and Modeling Cell: Compendium of Material Composition Data for Radiation Transport Modeling*. U.S. Department of Homeland Security.

Romanenko, I., Holiuk, M., Kutsyn, P., Kutsyna, I., Odynokin, H., Nosovskyi, A., Gulik, V., 2019. New composite material based on heavy concrete reinforced by basalt-boron fiber for radioactive waste management. EPJ Nuclear Sciences & Technologies. https://doi.org/10.1051/epjn/2019050.

Romano, P. K., Horelik, N. E., Herman, B. R., Nelson, A. G., Forget, B., & Smith, K. (2015). OpenMC: A state-of-the-art Monte Carlo code for research and development. *Annals of Nuclear Energy*, *82*. https://doi.org/10.1016/j.anucene.2014.07.048

Skarżyński, Ł. (2020). Mechanical and radiation shielding properties of concrete reinforced with boron-basalt fibers using Digital Image Correlation and X-ray micro-computed tomography. *Construction and Building Materials*, *255*. https://doi.org/10.1016/j.conbuildmat.2020.119252

Soni, B. K., Makwana, R., Mukherjee, S., Barala, S. S., Parashari, S., Chauhan, R., Jodha, A. S., & Katovsky, K. (2021). Novel concrete compositions for γ-rays and neutron shielding using WC and B4C. *Results in Materials*, *10*. https://doi.org/10.1016/j.rinma.2021.100177

Tohver, H., Slavickas, A., Holiuk, M., Krasņikovs, A., Mõtlep, R., Nováková, I., Vaišnoras, M., & Gulik, V. (2024). Assessing shielding material performance: benchmarking of Monte Carlo codes for oil shale and basalt-boron fiber concretes. *Nuclear Engineering and Design*, *417*. https://doi.org/10.1016/j.nucengdes.2023.112811

Tsardaka, E. C., Sougioultzi, K., Konstantinidis, A., & Stefanidou, M. (2023). Interpreting the setting time of cement pastes for modelling mechanical properties. *Case Studies in Construction Materials*, *19*. https://doi.org/10.1016/j.cscm.2023.e02364

Vaidotas, A. (2013). Waste Inventory for Near Surface Repository (NSR) – 13482. *Annual Waste Management Symposium, WM2013*.

Werner, C. J. (2017). *MCNP Users Manual - Code Version 6.2 (report LA-UR-17-29981)*. Los Alamos National Laboratory.

Wieselquist, W. A., Lefebvre, R. A., & Jessee, M. A. (2020). *SCALE Code System, ORNL/TM-2005/39, Version 6.2.4 (CCC-834)*. Oak Ridge National Laboratory.

Ipbüker, C., Nulk, H., Gulik, V., Biland, A., & Tkaczyk, A. (2015). Radiation shielding properties of a novel cement-basalt mixture for nuclear energy applications. *Nuclear Engineering and Design, 284*. https://doi.org/10.1016/j.nucengdes.2014.12.007

Zorla, E., Ipbüker, C., Biland, A., Kiisk, M., Kovaljov, S., Tkaczyk, A. & Gulik, V. (2017). Radiation shielding properties of high performance concrete reinforced with basalt fibers infused with natural and enriched boron. *Nuclear Engineering and Design, 313*. https://doi.org/10.1016/j.nucengdes.2016.12.029